# Structural Study of Electrochemically Deposited Cu on p-GaAs(100) in $H_2SO_4$ Solution by In Situ Surface-Sensitive X-ray Absorption Fine Structure Measurements

**Kazuhisa Tamura,[†] Hiroyuki Oyanagi,[‡] Toshihiro Kondo,[†] Michio Koinuma,[§] and Kohei Uosaki*,[†]**

*Physical Chemistry Laboratory, Division of Chemistry, Graduate School of Science, Hokkaido University, Sapporo 060-0810, Japan, and Electrotechnical Laboratory, Tsukuba, Ibaraki, 305-8568, Japan*

*Received: March 27, 2000*

The local structures of electrochemically deposited Cu on p-GaAs(100) of various coverages in 0.1 M $H_2SO_4$ solution containing 0.1 mM $CuSO_4$ have been investigated by in situ surface-sensitive X-ray absorption fine structure (XAFS). The Cu K-edge extended X-ray absorption fine structure (EXAFS) and X-ray absorption near-edge structure (XANES) were obtained over a wide range of coverages, i.e., several monolayers down to 1/20 monolayer. The results of multishell parameter fitting of EXAFS data showed that Cu nanoclusters with a short Cu−Cu bond length were formed on the p-GaAs(100) electrode below the critical surface coverage of 0.25 monolayer. The nanoclusters were found to be coordinated with the oxygen atoms of water molecules and/or sulfate anions. They were formed in an early stage of electrochemical deposition and grew in size to approach a densely packed coordination with an fcc structure. XANES spectra showed that the coordination number changed systematically but that a metallic state was retained throughout the electrochemical deposition.

## 1. Introduction

The metal/semiconductor interface has been a subject of intensive studies because of its importance in modern device technology and scientific interests such as understanding of the microscopic mechanism of band bending or Schottky barriers. The electrochemical behavior of semiconductor electrodes has been investigated from 1955 when the semiconductor was invented.[1] More significant investigations of semiconductor electrodes have been carried out since the 1970s, triggered by the work of Fujishima and Honda[2] and the first energy crisis, because the semiconductor/electrolyte interface was considered to be useful for the conversion of solar energy to chemical energy, hydrogen, and/or electricity. The electrochemical characteristics of semiconductors[3−8] are also important because they provide useful information about the wet-type processing of semiconductors such as etching and metal deposition.

A large number of studies has been carried out to understand the mechanism of electrochemical deposition of metal on conducting surfaces because of the great technological importance.[9−11] To fully understand the deposition process, it is essential to elucidate the local structure of the substrate and the deposited overlayer on an atomic scale.[12−16] Although the structures of electrochemically deposited Cu on metal have already been investigated by many research groups,[17−22] only a few studies on the electrochemical deposition of Cu on semiconductor electrodes have been carried out.[23−29]

GaAs is one of the most attractive semiconductor materials used in various electronic devices and dry/wet solar cells.[30−36] Scherb and Kolb[23] determined the amounts of electrochemically deposited Cu on n-GaAs(100) by photoreflectivity measurement. Vereecken et al.[24] reported the electrochemical behavior of both n- and p-type GaAs(100) in electrolyte solutions containing Cu. We have investigated the structure of electrochemically deposited Cu on GaAs(100) with various coverages using atomic force microscopy (AFM) and optical methods and found that Cu clusters were formed in an early stage and grew in size.[26,27] AFM can, however, provide structural information only on the top layer, but the structure of the deposit/substrate interface cannot be obtained. Furthermore, the spatial resolution of AFM is on the order of ångstroms, while the bond length should be determined within 0.1 Å in order to understand the nature of the chemical bond. Surface X-ray scattering (SXS), which can provide information on the average structure with higher resolution, has recently been applied to semiconductor/electrolyte solution interfaces by Zegenhagen et al.[25,28,29] and by us.[29,37] SXS also has some limitations because a well-ordered surface structure is required for the application.

X-ray absorption fine structure (XAFS) can overcome these limitations as it can provide detailed information about the local structure and the electronic structure of atoms with high sensitivity even at the surface without a long-range order.[38,39] XAFS consists of two regions, extended X-ray absorption fine structure (EXAFS) with a typical energy range of 1 keV and X-ray absorption near-edge structure (XANES) observed within 50 eV above the threshold. EXAFS is based on an interference phenomenon of photoelectrons, which occurs between the outgoing waves and the scattered waves. On the other hand, XANES is caused by a bound-state transition and multiple scattering resonances of photoelectrons and, therefore, is sensitive to the electronic state of an absorbing atom and the coordination geometry. For normal incidence geometry in a hard X-ray region, both the penetration depth of the incident X-ray and the escape depth of a fluorescent X-ray are much greater than the thickness of a typical surface layer that we are interested in (<3 Å). Below a critical angle, however, the X-ray is totally

* To whom correspondence should be addressed. E-mail: uosaki@pcl.sci.hokudai.ac.jp.
[†] Hokkaido University.
[‡] Electrotechnical Laboratory.
[§] Present address: Department of Applied Chemistry and Biochemistry, Faculty of Engineering, Kumamoto University, Kurokami, Kumamoto 860, Japan.

10.1021/jp0011286 CCC: $19.00 
Published on Web 08/31/2000

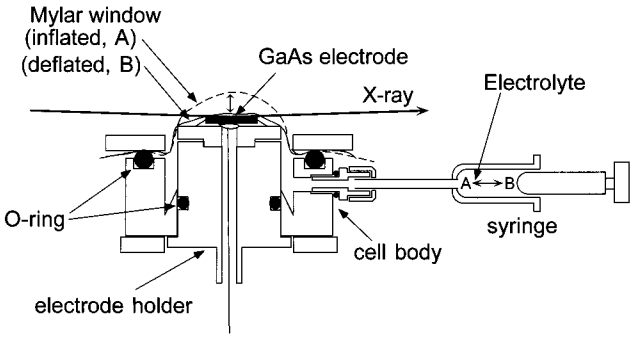


**Figure 1.** Side view of spectroelectrochemical cell for grazing incident XAFS measurement.

reflected as it crosses the interface between the two media and, therefore, the extinction length is reduced by several orders of magnitude.[40] Thus, submonolayer surface sensitivity has been achieved using a grazing-incidence geometry.[41,42] Although X-ray techniques can be used even in solution because hard X-rays have a great penetration depth in an aqueous solution, only a few publications are available on the application of XAFS to electrode/electrolyte interfaces.[17,38,43−46] We have carried out XAFS studies on GaAs electrode/electrolyte interfaces, and preliminary results have been reported.[47,48]

In this paper, we report the detailed analysis of XAFS data for electrochemically deposited Cu of various thicknesses on p-GaAs(100) and discuss the growth mechanism of Cu overlayers, particularly at the initial deposition stage. EXAFS data showed that Cu nanoclusters characterized by a shorter Cu−Cu bond length than that of the fcc Cu were formed when the surface coverage, $\theta$, of the Cu overlayer was less than 0.25 monolayer (ML). The Cu microclusters with an fcc structure appeared at higher coverage. Cu atoms in nanoclusters were coordinated with the O atoms of a water molecule and/or a sulfate anion. XANES spectra indicate that the Cu overlayers consisted of Cu metal not Cu cations at all coverages investigated in this study.

## 2. Experimental Section

**2.1. Materials and Electrochemical Measurements.** Reagent grade $H_2SO_4$, $CuSO_4$, acetone, and ethanol were obtained from Wako Pure Chemicals and used without further purification. Ultrapure water was obtained by a Milli-Q water purification system (Yamato, WQ-500).

Single crystalline Zn-doped p-GaAs(100) wafers (Mitsubishi Chemical Corp., doping density $1.0 \times 10^{19}$ cm$^{-3}$) were used as electrodes. Samples were cleaned in hot acetone and then in ethanol, dipped in 3 M HCl to remove the surface oxide, and rinsed with pure water before each measurement. Ohmic contact was secured using an In−Zn alloy. The GaAs sample was fixed on a sample holder, which was made from polychlorotrifluoroethylene (PCTFE), using an epoxy resin, and then was placed in a specially designed electrochemical cell made from PCTFE (Figure 1). A 6.0 $\mu$m thick polyethylene film (Chemplex, Mylar 250) was used as a window. The electrode potential was controlled by a potentiostat (Hokuto Denko, HA151) with respect to an Ag/AgCl electrode connected to the cell through a capillary tube. The counter electrode was a Pt wire.

**2.2. Surface-Sensitive XAFS Measurements.** X-ray absorption experiments were carried out in the fluorescence mode with a grazing-incidence geometry (incidence angle was set at 0.4−1.6°). A multipole wiggler (MPW) magnet inserted in a straight section of the 2.5 GeV storage ring (BL13B) at the Photon Factory of High Energy Accelerator Research Organization was used as a light source. The electrical field vector of the incident beam was parallel to the electrode surface. A maximum magnetic field, $B_0$, of 1.5 T (total power: 5.44 kW) provided a high flux greater than that of a bending magnet by an order of magnitude extending over a wide energy range (4−30 keV). Using a directly water-cooled Si(111) double crystal monochromator,[49] an energy resolution of $\Delta E/E \sim 2 \times 10^{-4}$ was obtained for $B_0 < 1.25$ T. The beam size was 50 $\mu$m (vertical) $\times$ 10 mm (horizontal). Cu K edge fluorescence was monitored using a 19-element pure Ge solid-state detector (SSD),[50] and its intensity was normalized by the incident X-ray intensity, $I_0$, which was monitored by an ionization chamber filled with nitrogen gas. To remove background X-rays, a Ni filter was placed in front of the Be window of the SSD. The energy of the incident X-ray was calibrated to the Fermi level (8.9803 keV) of Cu. The total data acquisition time for one spectrum was about 2−3 h, and all channel data were recorded separately and averaged out after repeating several scans.

An electrolyte solution of 0.1 M $H_2SO_4$ containing 0.1 mM $CuSO_4$ was introduced into the electrochemical cell under potential control at +0.1 V, where no current was observed; i.e., both the electrochemical deposition of Cu and the anodic dissolution of GaAs did not take place. Electrochemical deposition of Cu was carried out by stepping the potential from +0.1 V to −0.5 V and keeping it at −0.5 V for certain time periods while maintaining the thickness of the solution between the electrode and the window at more than 5 mm. To terminate deposition, the electrode potential was stepped to −0.35 V and, at the same time, the solution thickness was decreased to less than several tens of micrometers by deflation. When the solution thickness was kept at less than several tens of micrometers at −0.35 V, neither cathodic deposition current nor anodic dissolution current was observed because of the large IR drop. This arrangement has another advantage of minimizing the scattering of X-rays by the solution. The $\theta$ of the Cu overlayers was estimated to be 0.05, 0.08, 0.17, 0.25, 1, and 6 ML for deposition times of 1 s, 5 s, 30 s, 1, 10, and 30 min, respectively, from the charge of the anodic dissolution of Cu, which was carried out after the X-ray measurements with the solution thickness increased to 5 mm by introducing electrolyte.

XAFS spectra of Cu foil, $Cu_2O$, and CuO powders were obtained as references in a transmission mode.

## 3. EXAFS Data Analysis

The first step of data analysis is the elimination of the background functions due to atomic absorption. A smooth background function was generated by a cubic spline function normalized at the absorption edge so that the subtracted part varied with energy according to the Victoreen equation.[51] Assuming that the preedge part and the postedge part, if EXAFS oscillations are averaged out, follow the energy dependence given by the Victoreen function, we generated the unknown background function so that the subtracted part becomes a function of $\lambda^{-3}$ and $\lambda^{-4}$, where $\lambda$ indicates the wavelength of the X-ray. The smooth background absorption of a free atom, $\mu_0$, was estimated by a cubic spline function with five knots. After the subtraction of $\mu_0$ and normalization with $\mu_0$, a familiar expression of EXAFS oscillations as a function of photoelectron wavenumber $k$, $\chi(k)$, was obtained. The initial zero in energy used in a conversion of energy scale was taken as the absorption inflection point of a sharp feature at 8.9803 keV of the near-edge spectrum of Cu metal.

The $\chi(k)$ within a single scattering theory can be described by the following formula[52]

$$\chi(k) = \Sigma(N_i/kR_i^2)F_i(k,\pi)\sin(2kR_i + \Phi_i)e^{-2\sigma_i^2k^2}e^{-2R_i/\lambda_i} \quad (1)$$

where $k$ is the photoelectron wavenumber, $N_i$ is the coordination number of the $i$th shell, $R_i$ is the interatomic distance, $F_i(k,\pi)$ is the backscattering amplitude, $\Phi_i$ is the total phase shift, $\sigma_i^2$ is the mean-square relative displacement (MSRD), and $\lambda_i$ is the mean free path of the photoelectron. The energy variation, $\Delta E_0$, is introduced to correct the zero energy of a muffin tin potential,[53]

$$k' = (k^2 - 2m\Delta E_0/\hbar^2)^{1/2} \quad (2)$$

where $k'$ is the corrected wavenumber and $m$ is the electron mass. The structural parameters such as $R_i$, $N_i$, $\sigma_i^2$, and $\Delta E_{0i}$ are obtained by the analysis of the EXAFS oscillations, and in some cases, atomic species can be determined from the EXAFS envelope because the $k$ dependence of $F_i(k,\pi)$ strongly depends on the atomic number, $Z$. The adjustment of the energy scale was done by introducing a correction parameter $\Delta E_0$. To relate $\chi(k)$ to radial distribution, EXAFS oscillations are Fourier transformed by a standard procedure. Using Fourier filtering of the peaks in Fourier transform (FT), the contribution of a particular shell can be separated also. The analysis of the $k$-weighted EXAFS oscillations, $k\chi(k)$, was carried out over a range of $k$ between 4.0 and 12.0 Å$^{-1}$. The least-squares parameter fitting based on Marquart's scheme[54] for iterative estimation of nonlinear least-squares parameters via a compromise combination of gradient and Taylor series method was used to fit the Fourier filtered $\chi(k)$. The interactive parameter fitting code was developed using C language and with a graphic user interface on a UNIX operating system[55] on the basis of the TSS-based FORTRAN 77 code.[56]

The effect of Zn Kα excitation cannot be neglected in the higher $k$ region, and $\chi(k)$ damps its magnitude sharply as $k$ increases; therefore the least-squares parameter fitting in the present study was carried out in a limited range of $k$. For a high $\theta$ region ($\theta$ = 1 and 6 ML), the parameter fitting was performed for a single shell because only one dominant peak was observed in the FT. For a low $\theta$ region ($\theta$ = 0.05, 0.08, 0.17, and 0.25 ML), the parameter fitting was performed for two or three shells, because two or three peaks were observed in the FT. To retain the criterion on the degrees of freedom in parameter, some of the parameters were fixed, as will be described in the next section. Under all the fitting conditions, the number of parameters was less than the degrees of freedom, $2\Delta k\Delta R/\pi$.[57]

## 4. Results

Figure 2 shows a cyclic voltammogram of a p-GaAs(100) electrode obtained in a solution containing 0.1 M $H_2SO_4$ and 0.1 mM $CuSO_4$ with a scan rate of 20 mV s$^{-1}$. In the negative scan, cathodic current flowed at a potential more negative than −0.05 V, and a relatively broad cathodic peak was observed around −0.15 V. In the positive scan, a sharp anodic current peak was observed at +0.03 V. The cathodic current is assigned to the electrochemical deposition of Cu onto the GaAs surface, the anodic peak corresponds to the dissolution of the electrochemically deposited Cu. At +0.2 V, which is more negative than the flat-band potential of p-GaAs (+0.32 V)[58] at this pH, the anodic current due to the anodic dissolution of GaAs electrode started to flow.[27]

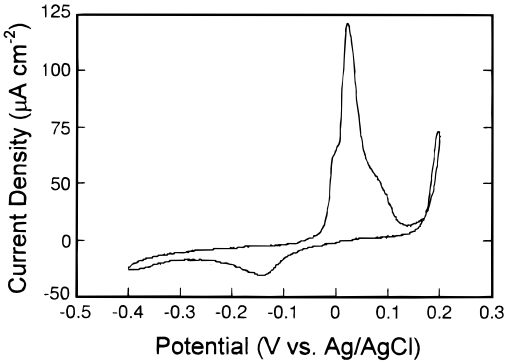


**Figure 2.** Cyclic voltammogram of p-GaAs(100) electrode in 0.1 M $H_2SO_4$ and 0.1 mM $CuSO_4$ solution. Sweep rate: 20 mV s$^{-1}$.

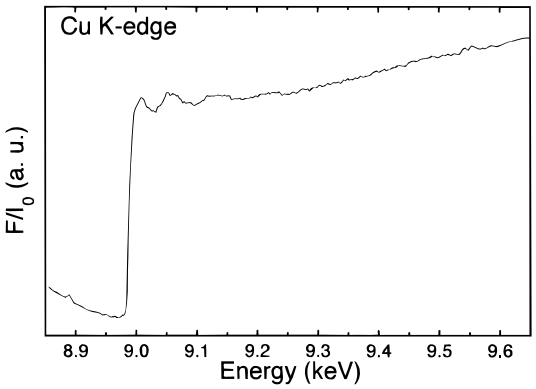


**Figure 3.** Cu K edge fluorescence yield (EXAFS) spectrum of Cu/p-GaAs(100) measured at 0 V in 0.1 M $H_2SO_4$ and 0.1 mM $CuSO_4$ solution: Cu was electrochemically deposited at −0.5 V for 5 s. Fluorescence yield, $F$, is normalized by $I_0$.

Figure 3 shows a typical fluorescence yield spectrum for Cu overlayers deposited on a p-GaAs(100) electrode, which was obtained after the potential was kept at −0.5 V for 5 s in 0.1 M $H_2SO_4$ solution containing 0.1 mM $CuSO_4$. This spectrum shows a high signal-to-background (S/B) ratio despite the very small Cu concentration on the GaAs surface, i.e., $\theta$ = 0.05 ML in this case. Such a high surface sensitivity is achieved by a 19-element pure Ge SSD[50] and a grazing-incidence geometry for fluorescence excitation.[41] Above the K-shell absorption edge (8.98 keV), the fluorescence yield reflects the modulations in the absorption cross section over a wide energy range due to EXAFS.

Figures 4 and 5 show the normalized EXAFS oscillations $\chi(k)$ as a function of $k$ and the FT as a function of $R$, respectively, for six specimens, i.e., Cu overlayers on the p-GaAs electrode with various $\theta$ values. The FT for the Cu foil data is also shown in Figure 5g as a reference. The FT range in the $k$ space was 3.5−12.4 Å$^{-1}$ for 0.05, 0.08, 0.17, and 0.25 ML, 3.3−13.4 Å$^{-1}$ for 1 ML, and 3.6−12.3 Å$^{-1}$ for 6 ML. For $\theta$ = 0.05, 0.08, and 0.17 ML (Figure 5a−c, respectively), two peaks, A at 1.37 Å and B at 1.87 Å, were observed. For peak A, the EXAFS envelope extracted by back-Fourier transform of $k^3\chi(k)$ falls off sharply with an increase in $k$, indicating that the coordinated atom is a light element (low $Z$). There are sulfate anions and water molecules, which have light element atoms such as S, O, and H in the electrolyte. From the structural point of view, the most likely atom that coordinates to Cu atoms of nanoclusters is an oxygen atom. Thus, peak A is ascribed to the Cu−O bond. The envelope of filtered EXAFS for peak B has a maximum at $k$ = 6.2 Å$^{-1}$, indicating that the scattering atomic species are Cu, Ga, or As atoms, which would give a similar $k$ dependence. On the basis of the fact that the

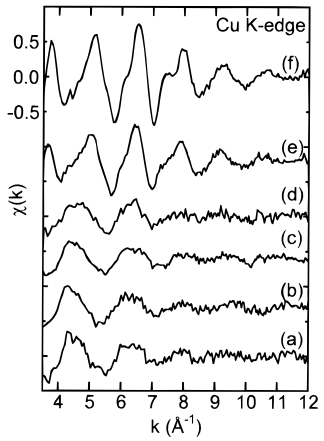


**Figure 4.** Cu K-EXAFS oscillations of Cu/p-GaAs(100) in 0.1 M $H_2SO_4$ and 0.1 mM $CuSO_4$ solution plotted as a function of photoelectron wavenumber, *k*. Cu was electrochemically deposited at −0.5 V for (a) 0.05 ML, (b) 0.08 ML, (c) 0.17 ML, (d) 0.25 ML, (e) 1 ML, and (f) 6 ML.

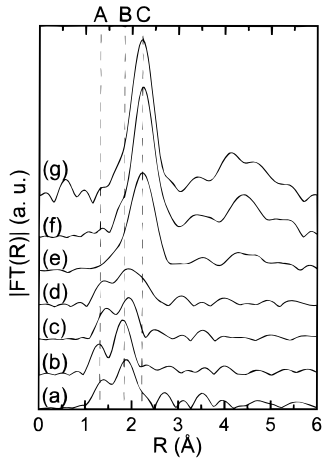


**Figure 5.** Fourier transforms of Cu K-EXAFS oscillations for (a) 0.05 ML, (b) 0.08 ML, (c) 0.17 ML, (d) 0.25 ML, (e) 1 ML, and (f) 6 ML, and (g) Cu foil. The phase shift is not corrected.

electrical field vector was parallel to the electrode surface, peak B should be ascribed to the Cu−Cu bond, which is found as a dominant bond in fcc-like clusters.

For $\theta = 0.25$ ML (Figure 5d), in addition to the above-mentioned two peaks (A at 1.37 Å, B at 1.87 Å), a new shoulder feature C was observed at 2.25 Å. Here peaks A and B can be ascribed to the Cu−O and Cu−Cu bonds, respectively, because they were observed at the same position for the samples with $\theta = 0.05$, 0.08, and 0.17 ML. For shoulder C, we cannot filter the EXAFS oscillations as a single peak because of limited resolution in the *R* space. However, because peak C is located at the same position of the Cu−Cu bond in Cu metal with an fcc structure, as shown in Figure 5g, the shoulder C can be ascribed to the Cu−Cu bond with an fcc-like geometry. For $\theta \geq 1$ ML, a dominant peak C was observed (Figure 5e,f) at the same position of the shoulder C (2.23 Å) in Figure 5g. Because the EXAFS envelope at peak C had a maximum at 6.3 Å$^{-1}$, peak C can be ascribed to the Cu−Cu bond with a closely packed fcc Cu.

To investigate the structure of electrochemically deposited Cu on the p-GaAs electrode in more detail, least-squares parameter fitting was carried out. The ranges in the *R* space used for Fourier filtering of the FT were 0.86−2.46, 0.95−2.25, 1.00−2.25, 1.06−2.70, 1.00−2.80, and 1.48−2.92 Å for the $\theta = 0.05$, 0.08, 0.17, 0.25, 1, and 6 ML, respectively.

**TABLE 1: Values of *R*, *N*, $\sigma$, and $\Delta E_0$ Obtained by Parameter Fitting of X(*k*) with Various $\theta$**

| $\theta$ (ML) | bond type | *R* (Å) | *N* | $\sigma$ (Å$^{-1}$) | $\Delta E_0$ (eV) |
|---|---|---|---|---|---|
| 0.05 | Cu−O | 1.85 ± 0.04 | 2.1 ± 0.4 | 0.037 ± 0.03 | 5.13[a] |
| | Cu−Cu | 2.08 ± 0.03 | 2.5 ± 1.0 | 0.086 ± 0.02 | 3.61[a] |
| 0.08 | Cu−O | 1.85 ± 0.06 | 1.1 ± 0.8 | 0.037[a] | 5.13[a] |
| | Cu−Cu | 2.07 ± 0.02 | 2.4 ± 0.8 | 0.086[a] | 3.61[a] |
| 0.17 | Cu−O | 1.86 ± 0.06 | 0.9 ± 0.8 | 0.037[a] | 5.13[a] |
| | Cu−Cu | 2.05 ± 0.03 | 1.8 ± 0.8 | 0.086[a] | 3.61[a] |
| 0.25 | Cu−O | 1.96 ± 0.03 | 1.7 ± 0.5 | 0.037[a] | 5.13[a] |
| | Cu−Cu | 2.10 ± 0.04 | 0.5 ± 0.4 | 0.086[a] | 3.61[a] |
| | Cu−Cu | 2.56 ± 0.03 | 2.1 ± 0.7 | 0.084[a] | 3.61[a] |
| 1 | Cu−Cu | 2.55 ± 0.02 | 8.6 ± 1.9 | 0.083 ± 0.01 | 3.61[a] |
| 6 | Cu−Cu | 2.52 ± 0.01 | 11.6 ± 1.1 | 0.084 ± 0.01 | 3.61[a] |

[a] Fixed value in the parameter fitting.

For $\theta \geq 1$ ML, the FT had the dominant peak C at 2.23 Å, which was ascribed to Cu−Cu in an fcc structure. Thus, a single shell least-squares fit can be performed to obtain *N*, $\sigma$, and *R*. We fixed the value of $\Delta E_0$ to be 3.61 eV, which was obtained from the analyses of Cu foil, because no energy shift in the absorption threshold was observed between the Cu overlayers and the Cu foil.

For $\theta = 0.05$, 0.08, and 0.17 ML, we performed a two-shell least-squares fit because FT (Figure 5a−c) had the two peaks at 1.37 (A) and 1.87 Å (B), which were assigned to the Cu−O and Cu−Cu contributions, respectively. To avoid the number of parameters exceeding the degrees of freedom, we fixed the value of $\Delta E_0$ for A and B to be 5.13 and 3.61 eV, respectively, which were obtained from analyses of CuO powder and Cu foil, respectively.

For $\theta = 0.25$ ML, because three peaks were obtained in FT (Figure 5d), we performed a three-shell fit. To limit the number of parameters within the degrees of freedom, we fixed the $\sigma$ and $\Delta E_0$ values for A, B, and C. The $\sigma$ and $\Delta E_0$ values used in the fit were 0.037 Å$^{-1}$ and 5.13 eV, 0.086 Å$^{-1}$ and 3.61 eV, and 0.084 Å$^{-1}$ and 3.61 eV obtained from the results of fit for the data with $\theta = 0.05$, 0.08, and 6 ML, respectively.

The fitted $\chi(k)$ and results of FT are shown in Figures 6 and 7, respectively, and the structural parameters obtained by a least-squares fit are summarized in Table 1.

The absorption edge energy in the XANES spectra reflects the electronic state of the excited atom. Thus, the information on valency is easily obtained by comparing the absorption edge energy with reference compounds. For Cu oxides and metal, a systematic blue energy shift is observed on going from a metal (0) to $Na_2CuO_3$ (+3). Figure 8 shows the XANES spectra and their derivative for the Cu overlayers on the p-GaAs electrode with various $\theta$ values, together with those of Cu foil, $Cu_2O$, and CuO as references. The Fermi energy in the derivative of the XANES spectra (inflection point of the first peak of absorption edge) was compared. The Fermi energy of the Cu K-shell for the references was observed at 8.9803 keV for Cu foil ($Cu^0$: Figure 8g), 8.9831 keV for $Cu_2O$ ($Cu^+$: Figure 8h), and 8.9847 keV for CuO ($Cu^{2+}$: Figure 8i). These values of edge energy matched well with literature values.[59] The Fermi energy of the electrochemically deposited Cu on the GaAs electrode appeared at 8.980 keV for all $\theta$ values, indicating that the valency of the electrochemically deposited Cu is 0 and is not dependent on $\theta$. The two peaks at 15 and 25 eV above the absorption edge were observed only for $\theta \geq 0.25$ ML. These two peaks were reported to be affected by the contribution of the multiple scattering with an fcc structure,[60] indicating that the Cu overlayers of $\theta \geq 0.25$ ML have an fcc structure. Thus,

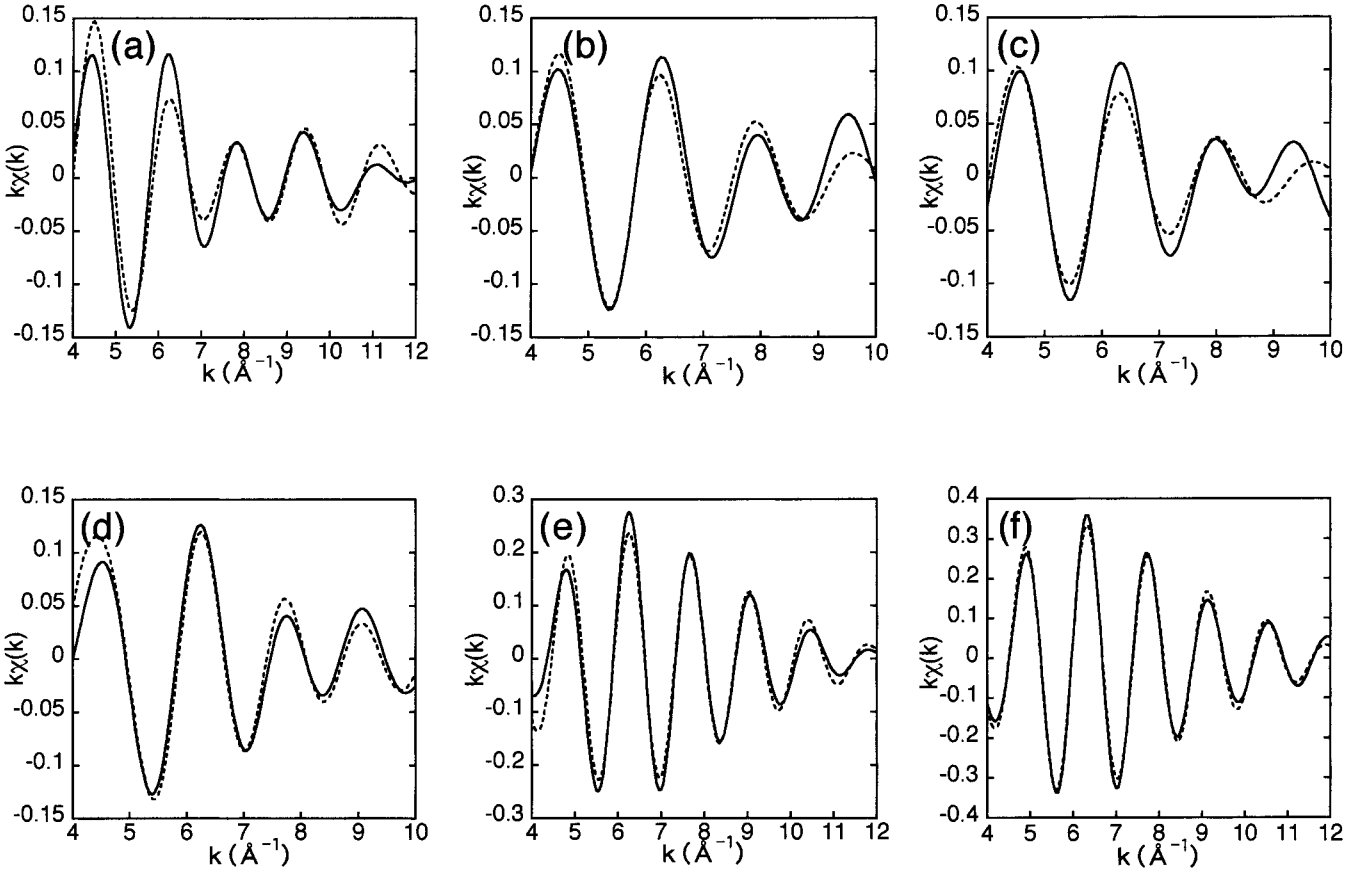


**Figure 6.** Curve fit results of Fourier filtered $k\chi(k)$. All the samples were as Figure 4. The solid line is the experimental data and the dotted line is the fitting data.

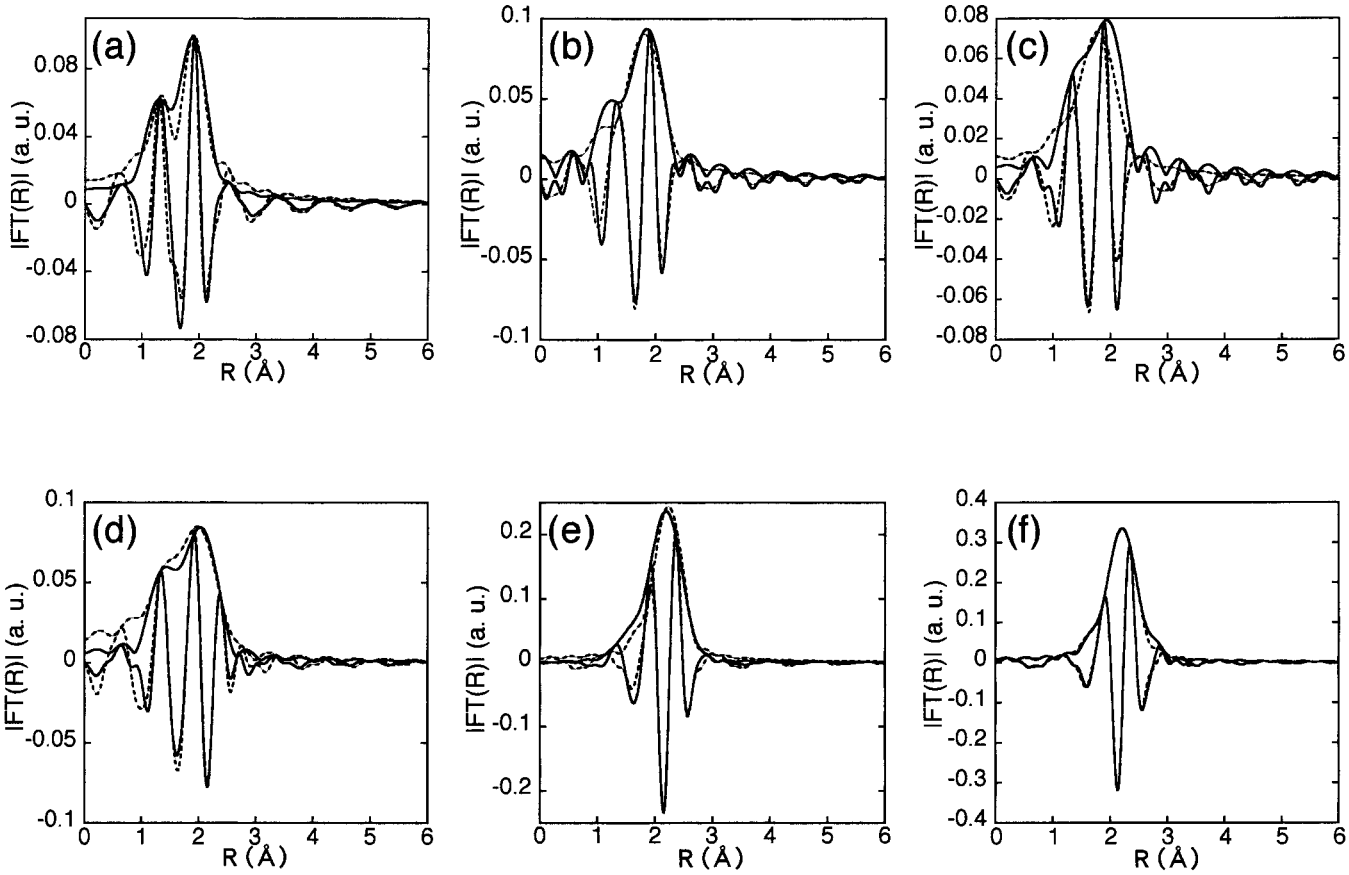


**Figure 7.** Curve fit results of Fourier transforms. All the samples were as Figure 4. The solid line is the experimental data and the dotted line is the fitting data.

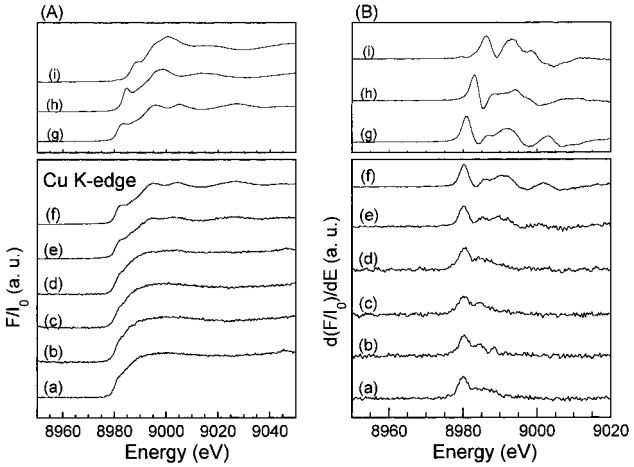


**Figure 8.** Cu K-XANES spectra of Cu/p-GaAs(100) for (a) 0.05 ML, (b) 0.08 ML, (c) 0.17 ML, (d) 0.25 ML, (e) 1 ML, and (f) 6 ML and (g) Cu foil, (h) $Cu_2O$, and (i) CuO. (A) is the experimental data and (B) is the differential of experimental data.

the Cu overlayers with an fcc structure start to grow when $\theta$ exceeds 0.25 ML, which is in agreement with the results of EXAFS analysis.

## 5. Discussion

As described before, when $\theta = 0.05$, 0.08, and 0.17 ML, there were two components in the main peak with different backscattering atoms, i.e., Cu−Cu and Cu−O. The results summarized in Table 1 show that the Cu−Cu distance and the coordination number for this bonding at these coverages are much shorter and smaller than those of Cu metal whose Cu−Cu distance and the coordination number are 2.56 Å and 12, respectively. Montano et al. reported that the interatomic distance of a Cu dimer prepared by the gas-aggregation technique is as small as 2.23 Å.[61,62] Katagiri et al. calculated the interatomic distance of the Cu clusters using the embedded-atom method based on the density functional theory and found that the interatomic distance decreases with a decrease in the cluster size as 2.17 Å for a dimer, 2.26 Å for a trimer, and 2.31 Å for a tetramer.[63] The contracted Cu−Cu distances of 2.05−2.08 Å obtained in the present study for low coverage are slightly smaller than the above values. It can be concluded that the nanoclusters with shorter bond lengths such as dimers, trimers, and/or tetramers are formed on the p-GaAs(001) surface at an early stage of the electrochemical deposition of Cu. The observed small average coordination numbers for $\theta \leq 0.25$ ML also support the formation of Cu nanoclusters with the presence of a large disorder. It is well-known that the effect of large disorder causes an apparently shorter bond length because of an anharmonic term in the phase shift.[64]

The results of parameter fitting showed that O atoms, which should be in a water molecule and/or sulfate anion, coordinate to the nanoclusters. Tadjeddine et al. reported that the Cu−O distances for 1 ML Cu on Au(100) and 0.3 ML Cu on Au(111)[18] in sulfate solution are 1.99 and 1.95 Å, respectively.[17] Abruña et al. also reported that the Cu−O distance for 0.5 ML of Cu on Pt(111) in 0.1 M $H_2SO_4$ solution is 1.99 Å.[20] The Cu−O distance of 1.85 Å obtained in the present study (Table 1) is shorter than the reported values by 0.14 Å. Although it is nearly as short as the covalent bonds of CuO and $Cu_2O$, the XANES spectra (8.98 keV) show that electrodeposited Cu has a metallic character even at a very initial stage. We suppose that the electronic structure of Cu nanoclusters is different from that of bulk Cu and that it causes the contraction of the Cu−O bond. Such a deviation in bond length may arise from the anharmonicity of the Cu−O bond,[65] but because of a limitation in the number of free parameters, we did not analyze a higher order correction in this work.

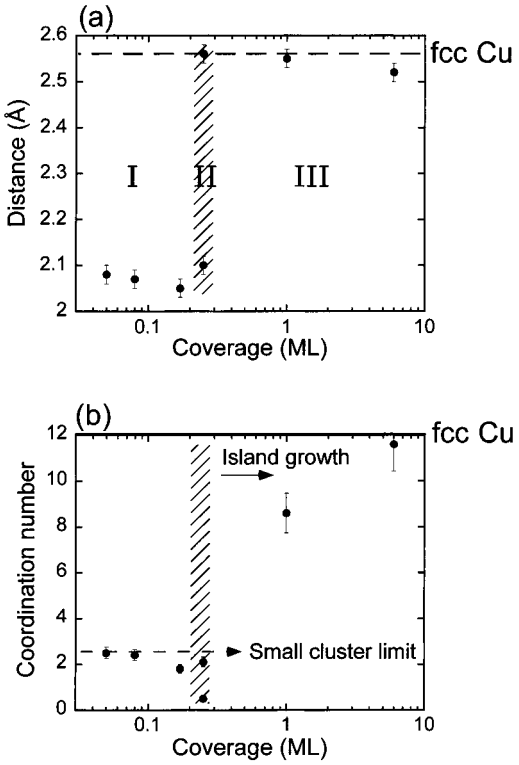


**Figure 9.** Dependence of bond length (a) and average coordination number (b) on nominal coverage for copper layers electrochemically deposited on the GaAs(100) electrode.

At $\theta = 0.25$ ML, in addition to the contracted Cu−Cu distance of 2.10 Å and the contracted Cu−O distance of 1.96 Å, the Cu−Cu distance of 2.56 Å was also observed. Peak C corresponds to that of the nearest neighbor atom in the Cu metal.[66] This result indicates that the microclusters begin to grow when the deposition exceeds a critical coverage, i.e., $\theta = 0.25$ ML, suggesting that nanoclusters are initially formed until they reach a certain density limit.

The analysis of EXAFS oscillations contributing to peak C in Figure 5 showed that the Cu−Cu distances at $\theta = 1$ and 6 ML are 2.55 and 2.52 Å, respectively. These values are in good agreement with that of Cu metal, i.e., 2.56 Å.[66] The average coordination number (8.6 and 11.6 for $\theta = 1$ and 6 ML, respectively) increases with the increase in $\theta$ approaching that of an fcc structure, i.e., 12, indicating that the microclusters are formed as the deposition proceeds beyond the critical coverage.

Figure 9 summarizes the Cu−Cu distance and average coordination number of Cu atoms as a function of $\theta$. Two distinct Cu−Cu distances were found in regions I and III. In the intermediate region II (shaded in Figure 9a), both of the two distinct distances were found. We simply observe the fraction-weighted average of coordination number in regions II and III; therefore, the contribution from the fcc-like Cu clusters dominates the EXAFS oscillations. Thus, it is difficult to analyze the EXAFS oscillation in region III using a two-domain model. However, because the bond lengths corresponding to these two domains are simultaneously observed in region II, it is concluded that the nanoclusters are initially formed, then fcc-like Cu microclusters are formed above the critical coverage ($\theta = 0.25$ ML) and grow in size as the coverage increases.

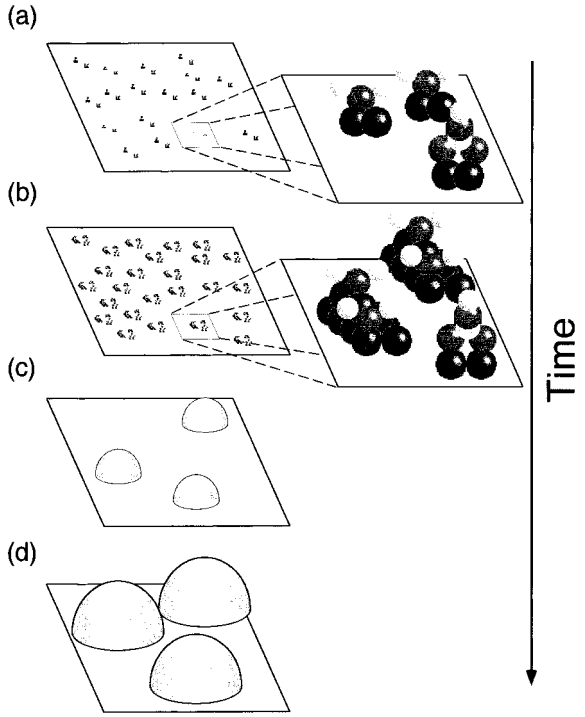


**Figure 10.** Proposed structural model of electrochemical deposition of Cu on GaAs in the initial stages for (a) $\theta \leq 0.17$ ML, (b) $\theta = 0.25$ ML, (c) $\theta = 1$ ML, and (d) $\theta = 6$ ML.

The present results are essentially in good agreement with our previous AFM,[26] in which we observed the Cu islands on flat terraces of the GaAs substrate at the initial stage of the Cu deposition. AFM studies have indicated that the Cu islands grew in size with deposition time but that the total number of the clusters was constant throughout the deposition. This implies that the size of each cluster increases as the coverage or the total amount of deposition increases. The present study, however, finds that in the initial stage, nanoclusters as a "nucleus" for 3D growth are formed with a unique short range order accompanied by the coordination of oxygen atoms. Figure 10 illustrates the schematic models of the local structures of electrochemically deposited Cu overlayers on the p-GaAs(100) electrode based on the present results and previous AFM studies. For $\theta \leq 0.17$ ML (Figure 10a), nanoclusters with a short Cu−Cu distance such as dimers, trimers, and/or tetramers are formed on the GaAs(100) surface, which are also coordinated with O atoms. In the higher coverage range ($\theta \geq 0.25$ ML), microclusters with an fcc structure are formed, but both nanoclusters and microclusters are present at the critical coverage value $\theta = 0.25$ ML (Figure 10b). The region between 0.25 and 1 ML is a transition region where the two clusters coexist. When $\theta$ exceeds 1 ML (Figure 10c and d), microclusters with an fcc structure dominate. The size of the microcluster with an fcc structure continues to increase with the deposition time.

## 6. Conclusions

The structures of the electrochemically deposited Cu on the p-GaAs(100) electrode were investigated by in situ surface-sensitive X-ray absorption fine structure (XAFS). Extended X-ray absorption fine structure (EXAFS) data showed that Cu nanoclusters with a short Cu−Cu distance such as dimers, trimers, and/or tetramers are formed on the p-GaAs surface at the initial stage ($\theta \leq 0.25$ ML). Above the critical coverage (0.25 ML), we found Cu microclusters, evidenced by a monotonic increase in coordination number having the Cu−Cu bond length for an fcc metal. X-ray absorption-near edge structure (XANES) spectra confirmed that electrochemically deposited metallic Cu exists throughout the coverage in the present study. The present results are essentially in good agreement with our previous AFM studies in which the nucleation of Cu atoms on the GaAs surface takes place at isolated places in the initial stage of electrochemical deposition. As a result of the consequent deposition of Cu atoms, islands are grown not on the bare GaAs surface but preferentially on the Cu nanoclusters. This should be due to the fact that the Cu−Cu interaction is stronger than Cu−Ga or Cu−As interactions.

**Acknowledgment.** We are grateful to Messrs. H. Fujita and H. Fujisawa of Mitsubishi Chemical Corp. for providing us with the GaAs single crystals. This work was partially supported by Grants-in-Aid for Scientific Research (No. 09740509) and on the Priority Area of "Electrochemistry of Ordered Interface (No. 09237101)" from the Ministry of Education, Science, Sports, and Culture, Japan, and the Yamada Science Foundation. X-ray measurements were performed under the approval of the Photon Factory Program Advisory Committee (PF-PAC No. 95G332 and 98G102). Dr. J. Zegenhagen is acknowledged for valuable comments and discussions.

## References and Notes

(1) Brattain, W. H.; Garrett, C. G. B. *Bell System Technol. J.* **1955**, *34*, 129.
(2) Fujishima, A.; Honda, K. *Nature* **1972**, *238*, 37.
(3) Gerischer, H. In *Physical Chemistry: An Advanced Treatise*; Eyring, H. Ed.; Academic Press: New York, 1970; Vol. IX, Chapter 5.
(4) Fujishima, A.; Kohayakawa, K.; Honda, K. *Bull. Chem. Soc. Jpn.* **1975**, *48*, 1041; *J. Electrochem. Soc.* **1975**, *122*, 1487.
(5) Gerischer, H. *J. Electroanal. Chem.* **1975**, *58*, 263.
(6) Morrison, S. R. *Electrochemistry at Semiconductors and Oxidized Electrode*; Plenum Press: New York, 1980.
(7) Pleskov, Y. V.; Gurevich, Y. Y. In *Semiconductor Photoelectrochemistry*; Bartlett, P. N., Ed.; Consultants Bureau: New York, 1986.
(8) Uosaki, K.; Kita, H. In *Modern Aspects of Electrochemistry*; White, R. E., Bockris, J. O'M., Conway, B. E., Eds.; Butterworth: London, 1986.
(9) Franaszczuk, K.; Sobkowski, J. *Surf. Sci.* **1988**, *204*, 530.
(10) Arvia, A. J.; Salvarezza, R. C.; Triaca, W. E. *Electrochim. Acta* **1989**, *34*, 1057.
(11) Markovic, N. M.; Ross, P. N., Jr. *J. Vac. Sci. Technol. A* **1993**, *11*, 2225.
(12) Eriksson, S.; Carlsson, P.; Holmström, B.; Uosaki, K. *J. Electroanal. Chem.* **1991**, *313*, 121.
(13) Thundat, T.; Nagahara, L. A.; Lindsay, S. M. *J. Vac. Sci. Technol. A* **1990**, *8*, 539.
(14) Itaya, K.; Sugawara, R.; Morita, Y.; Tokumoto, H. *Appl. Phys. Lett.* **1992**, *60*, 2534.
(15) Yau, S.-L.; Fan, F. F.; Bard, A. J. *J. Electrochem. Soc.* **1992**, *139*, 2825.
(16) Allongue, P.; Kieling, V.; Gerischer, H. *J. Electrochem. Soc.* **1993**, *140*, 1009.
(17) Tourillon, G.; Guay, D.; Tadjeddine, A. *J. Electroanal. Chem.* **1990**, *289*, 263.
(18) Tadjeddine, A.; Guay, D.; Ladouceur, M.; Tourillon, G. *Phys. Rev. Lett.* **1991**, *66*, 2235.
(19) Melroy, O. R.; Samant, M. G.; Borges, G. L.; Gordon, II, J. G.; Blum, L.; White, J. H.; Albarelli, M. J.; McMillan, M.; Abruña, H. D. *Langmuir* **1988**, *4*, 728.
(20) Bommarito, G. M.; Acevedo, D.; Rodrigues, J. F.; Abruña H. D. *J. Electroanal. Chem.* **1994**, *379*, 135.
(21) Sashikata, K.; Furuya, N.; Itaya, K. *J. Electroanal. Chem.* **1991**, *316*, 361.
(22) Kimizuka, N.; Itaya, K. *Faraday Discuss.* **1992**, *94*, 117.
(23) Scherb, G.; Kolb, D. M. *J. Electroanal. Chem.* **1995**, *396*, 151.
(24) Vereecken, P. M.; Kerchove, F. V.; Gomes, W. P. *Electrochim. Acta* **1996**, *41*, 95.
(25) Smilgies, D. M.; Feidenhans'l, R.; Scherb, G.; Kolb, D. M.; Kazimirov, A.; Zegenhagen, J. *Surf. Sci.* **1996**, *367*, 40.
(26) (a) Koinuma, M.; Uosaki, K. *Electrochim. Acta* **1995**, *40*, 1345. (b) Koinuma, M.; Uosaki, K. *J. Electroanal. Chem.* **1996**, *409*, 45.

(27) Tamura, K.; Kondo, T.; Uosaki, K. *J. Electrochem. Soc.* **2000**, in press.
(28) Zegenhagen, J.; Kazimirov, A.; Scherb, G.; Kolb, D. M.; Smilgies, D.-M.; Feidenhans'l, R. *Surf. Sci.* **1996**, *352*−*354*, 346.
(29) Scherb, G.; Kazimirov, A.; Zegenhagen, J.; Lee, T. L.; Noguchi, H.; Uosaki, K. *Phys. Rev. B* **1998**, *58*, 10800.
(30) Bockris, J. O'M.; Uosaki, K. *J. Electrochem. Soc.* **1977**, *124*, 1348.
(31) Frese, K. W., Jr.; Madou, M. J.; Morrison, S. R. *J. Electrochem. Soc.* **1981**, *128*, 1527.
(32) Allongue, P.; Cachet, H. *Electrochim. Acta* **1988**, *33*, 9.
(33) Plieth, W. J.; Pfuhl, G.; Felske, A.; Badawy, W. *Electrochim. Acta* **1989**, *34*, 1133.
(34) Uosaki, K.; Shigematsu, Y.; Kaneko, S.; Kita, H. *J. Phys. Chem.* **1989**, *93*, 6521.
(35) Uosaki, K.; Shigematsu, Y.; Kita, H.; Kunimatsu, K. *J. Phys. Chem.* **1990**, *94*, 4623.
(36) Hsieh, H. F.; Shih, H. C. *J. Electrochem. Soc.* **1991**, *138*, 1965.
(37) Uosaki, K.; Koinuma, M.; Kondo, T.; Ye, S.; Yagi, I.; Noguchi, H.; Tamura, K.; Takeshita, K.; Matsushita, T. *J. Electroanal. Chem.* **1997**, *429*, 13.
(38) Abruña, H. D. In *Electrochemical Interfaces; Modern Techniques for In-Situ Interface Characterization*; Abruña, H. D., Ed.; VCH: New York, 1991; Chapter 1.
(39) Teo, B. K. *EXAFS: Basic Principles and Analysis*; Springer-Verlag: Berlin, 1986.
(40) Becker, R. S.; Golovchenko, J. A.; Patel, J. R. *Phys. Rev. Lett.* **1983**, *50*, 153.
(41) Heald, S. M.; Keller, E.; Stern, E. A. *Phys. Lett.* **1984**, *A103*, 155.
(42) Oyanagi, H.; Sakamoto, K.; Shioda, R.; Kuwahara, Y.; Haga, K. *Phys. Rev.* **1995**, *B52*, 5824.
(43) Pandya, K. I.; Hoffman, R. W.; McBreen, J.; O'Grady, W. E. *J. Electrochem. Soc.* **1990**, *137*, 383.
(44) Davenport, A. J.; Isaacs, H. S.; Frankel, G. S.; Schrott, A. G.; Jahnes, C. V.; Russak, M. A. *J. Electrochem. Soc.* **1991**, *138*, 337.
(45) Druska, P.; Strehblow, H.-H. *J. Electroanal. Chem.* **1992**, *335*, 55.
(46) Yee, H. S.; Abruña, H. D. *J. Phys. Chem.* **1994**, *98*, 6552.
(47) Tamura, K.; Kondo, T.; Oyanagi, H.; Koinuma, M.; Uosaki, K. *J. Surf. Anal.* **1997**, *3*, 498.
(48) Kondo, T.; Tamura, K.; Koinuma, M.; Oyanagi, H.; Uosaki, K. *Chem. Lett.* **1997**, 761.
(49) Oyanagi, H.; Kuwahara, Y.; Yamaguchi, H. *Rev. Sci. Instrum.* **1995**, *66*, 4482.
(50) Oyanagi, H.; Martini, M.; Saito, M. *Nucl. Instrum. Methods* **1998**, *403*, 58.
(51) Victoreen, J. A. *J. Appl. Phys.* **1948**, *19*, 855.
(52) Saisho, H.; Goshi, Y. *Application of Synchrotron Radiation to Material Analysis*; Elsevier Science: New York, 1996; Chapter 4.
(53) Teo, B. K. *EXAFS*: *Basic Principles and Analysis*; Springer-Verlag: Berlin, 1986.
(54) Marquart, D. W. *J. Soc. Ind. Appl. Math.* **1963**, *11*, 431.
(55) Tamura, K.; Oyanagi, H.; Uosaki, K. Manuscript in preparation.
(56) Oyanagi, H. Unpublished.
(57) Lytle, F. W.; Sayers, D. E.; Stern, E. A. *Physica* **1989**, *B158*, 701.
(58) Kelly, J. J.; Memming, R. *J. Electrochem. Soc.* **1982**, *129*, 729.
(59) Oyanagi, H.; Oka, K.; Unoki, H.; Nishihara, Y.; Murata, K.; Yamaguchi, H.; Matsushita, T.; Tokumoto, M.; Kimura, Y. *J. Phys. Soc. Jpn.* **1989**, *58*, 2896.
(60) Yee, H. S.; Abruña, H. D. *Langmuir* **1993**, *9*, 2460.
(61) Montano, P. A.; Shenoy, G. K.; Alp, E. E.; Schulze, W.; Urban, J. *Phys. Rev. Lett.* **1986**, *56*, 2076.
(62) Apai, G.; Hamilton, J. F.; Stohr, J.; Thompson, A. *Phys. Rev. Lett.* **1979**, *43*, 165.
(63) Katagiri, M.; Miyamoto, A.; Coley, T. R.; Li, Y. S.; Newsam, J. M. *Mol. Simul.* **1996**, *17*, 1.
(64) Eisenberger, P.; Brown, G. *Sold State Commun.* **1979**, *29*, 481.
(65) Hung, N. V.; Frahm, R. *Physica B* **1995**, *208&209*, 97.
(66) Kittel, C. *Introduction to Solid State Physics*, 6th ed.; John Wiley & Sons: New York, 1986; p 24.